Analytical solutions of jam pattern formation on a ring for a class of optimal velocity traffic models

Gaididei, Yuri Borisovich; Berkemer, Rainer; Caputo, Jean Guy; Christiansen, P. L.; Kawamoto, Atsushi; Shiga, T.; Sørensen, Mads Peter; Starke, Jens

Published in:
New Journal of Physics

Link to article, DOI:
10.1088/1367-2630/11/7/073012

Publication date:
2009

Document Version
Publisher's PDF, also known as Version of record

Analytical solutions of jam pattern formation on a ring for a class of optimal velocity traffic models

2009 New J. Phys. 11 073012

(http://iopscience.iop.org/1367-2630/11/7/073012)

New Journal of Physics
The open-access journal for physics

Analytical solutions of jam pattern formation on a ring for a class of optimal velocity traffic models

Yu B Gaididei[1], R Berkemer[2], J G Caputo[3], P L Christiansen[4], A Kawamoto[5], T Shiga[5], M P Sørensen[2] and J Starke[2,6]

[1] Bogolyubov Institute for Theoretical Physics, Metrologichna str. 14 B, 01413, Kiev, Ukraine
[2] Department of Mathematics, Technical University of Denmark, DK-2800 Kongens Lyngby, Denmark
[3] Laboratoire de Mathématiques, INSA de Rouen, B.P. 8, 76131 Mont-Saint-Aignan cedex, France
[4] Department of Informatics and Mathematical Modeling and Department of Physics, Technical University of Denmark, DK-2800 Kongens Lyngby, Denmark
[5] Toyota Central R&D Labs, Inc., Nagakute Aichi, 480-1192, Japan
E-mail: galinag@mail.univ.kiev.ua, r.berkemer@mat.dtu.dk, caputo@insa-rouen.fr, plc@imm.dtu.dk, m.p.soerensen@mat.dtu.dk and j.starke@mat.dtu.dk

New Journal of Physics **11** (2009) 073012 (19pp)
Received 23 February 2009
Published 3 July 2009
Online at http://www.njp.org/
doi:10.1088/1367-2630/11/7/073012

Abstract. A follow-the-leader model of traffic flow on a closed loop is considered in the framework of the extended optimal velocity (OV) model where the driver reacts to both the following and the preceding car. Periodic wave train solutions that describe the formation of traffic congestion patterns are found analytically. Their velocity and amplitude are determined from a perturbation approach based on collective coordinates with the discrete modified Korteweg–de Vries equation as the zero order equation. This contains the standard OV model as a special case. The analytical results are in excellent agreement with numerical solutions.

[6] Author to whom any correspondence should be addressed.

Contents

1. Introduction

There is growing interest in the spatio-temporal behavior of highway traffic flow models (see [1]–[4]). It is now generally accepted that traffic flow can be considered as a particular example of collective non-equilibrium behavior of many-particle systems and that many collective phenomena such as non-equilibrium phase transitions, dynamical bifurcations and pattern formations are inherent features of traffic flow models. The collective character of traffic flow is due to vehicle–vehicle correlation effects originating from the interaction of drivers to avoid colliding with other moving vehicles and pedestrians. For example, a driver has to start braking early when the vehicle in front of him is too close.

There are several microscopic models aimed to describe the empirical observations in traffic flow dynamics. One can find very comprehensive descriptions of these models in review papers [2]–[6]. A comparative study of traffic flow models was also presented quite recently in [7]. One of the simplest but rich and widely used microscopic traffic flow models is the so-called optimal velocity (OV) model that was introduced in [8]. In the framework of this model the vehicles are ordered by their position, $s_n(t) \in \mathbb{R}$ at time t, such that $s_n(t) < s_{n+1}(t)$. Here, the subscript n denotes the car numbering. Each driver controls the acceleration to reduce the difference between the car velocity $\dot{s}_n$ and an optimal velocity (OV) $V(u_n(t))$, depending on the distance $u_n(t) := s_{n+1}(t) - s_n(t)$, i.e. the distance to the vehicle in front. Then the model is described by the differential equation

$$\tau\, \ddot{s}_n = V(u_n(t)) - \dot{s}_n, \quad n = 1, 2, \ldots, N, \tag{1}$$

where $\tau = 1/a$ is the relaxation time, its inverse a is called sensitivity and N is the total number of cars. The OV function V is typically chosen as $V(u) = (v_0/2)(\tanh(u - d) + \tanh(d))$ with d encompassing the car length plus a safety distance and v_0 being an upper limit of the velocity. In [9, 10], a relation between microscopic OV models and macroscopic (hydrodynamic) traffic models was established. The steady state solutions of hydrodynamic traffic models were analyzed in [11] and they correspond to a homogeneous flow, i.e. the cars are equidistant. When this solution becomes unstable traffic jams occur and propagate as density waves [8, 12, 13]. Starting from the hydrodynamic traffic model, Kurtze and Hung derived the

Korteweg–de Vries (KdV) equation possessing soliton solutions [14]. Based on the OV model, Komatsu and Sasa [15] were also able to derive the KdV equation, and the modified KdV equation was derived from a modified OV model by Ou *et al* [16]. In [17], the OV function is approximated by piecewise linear functions to simplify subsequent analysis.

To model real traffic situations with a high density of cars in the flow, the OV models are usually used on an infinite line or on a ring. The existence and stability conditions of a quasi-stationary free-way solution, when all cars move with the same velocity and have a constant headway, were studied in [18]–[20]. Numerical as well as analytical bifurcation analysis of a class of follow-the-leader traffic models was carried out in [21]–[23]. In [21], an OV model with a time lag was studied and multiple solutions and the presence of a subcritical Hopf bifurcation were established. In [22], a bifurcation analysis was carried out for a rather general class of OV functions $V(u)$, and it was proven that the loss of stability of the free-flow solution is generally due to a Hopf bifurcation. In [23], the bifurcation analysis was done and multiple traffic jams were obtained in a car-following model with reaction time.

In this paper, we investigate the traffic jam creation and propagation for the OV model on a ring. We study an extended OV model that was proposed in [24, 25] where a driver looks at the following car as well as at the preceding car. We develop an analytical approach that gives some insight into the mechanism of traffic jams.

The paper is organized as follows. In section 2, we present the model. In section 3, we shortly recall the known stability analysis. In sections 4 and 5, we derive a multi-jam traveling wave solution and find its velocity. In section 6, we compare the analytical results with the results of numerical simulations. Section 7 presents some concluding remarks.

2. Extended OV model

The equations for the car position $s_n(t)$ on a ring in the framework of the extended OV model have the form

$$\tau\,\ddot{s}_n + \dot{s}_n = V_{\mathrm{f}}(s_{n+1} - s_n) + V_{\mathrm{b}}(s_n - s_{n-1}), \qquad n = 1, 2, \ldots, N. \tag{2}$$

where N is the number of cars and the car position coordinates satisfy the periodicity condition

$$s_{n+N}(t) = s_n(t) + L, \tag{3}$$

where L is the length of the road. In equations (2), $V_{\mathrm{f}}(x)$ is a forward looking OV and $V_{\mathrm{b}}(x)$ is the backward looking OV and τ is the relaxation time. We will assume that the driver reacts to a decreasing distance as well as an increasing distance between his car and the car that is in front of him and take the forward looking OV in the form

$$V_f(x) = f\,\tanh(x - h), \tag{4}$$

as illustrated in figure 1.

Here h is the sum of the car length and safety distance between cars. The parameter $f \geqslant 0$ denotes the forward sensitivity of the model. We will also assume that the driver reacts to a change of the distance between his car and the car that is behind it and take the backward looking OV in the form

$$V_b(x) = -b\,\tanh(x - h). \tag{5}$$

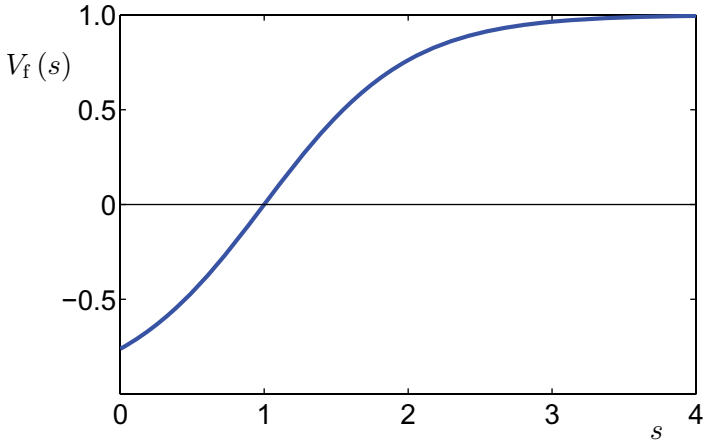

Figure 1. The forward looking OV profile $V_{\mathrm{f}}(s)$ given in (4) for $h = 1$, $f = 1$.

The parameter $b \geqslant 0$ gives the backward sensitivity and we use the same safety distance h as in the forward OV expression in (4).

3. Stability of the uniform free flow

An ideal and desired traffic flow is one with all cars moving with the same velocity $V(\ell)$ and keeping the same distance $\ell = L/N$ between nearest neighboring cars. We shall denote such a traffic flow uniform and it is the simplest possible traffic flow we can imagine. The question is under which conditions the uniform traffic flow is stable or not, anticipating that an unstable uniform flow will lead to traffic jams (refer also to results in [25, 26]). The uniform traffic flow solution of equations (2) reads

$$S_n(t) = n\,\ell + V(\ell)\,t \quad \text{with } V(\ell) = V_f(\ell) + V_b(\ell) + v, \tag{6}$$

which is a steady state solution on a ring with the total length L where v is the velocity of the frame of reference. Assuming that $s_n(t) = S_n(t) + \psi_n(t)$ and linearizing equations (2) with respect to $\psi_n(t)$ we obtain

$$\tau \frac{\mathrm{d}^2}{\mathrm{d}t^2}\psi_n(t) + \frac{\mathrm{d}}{\mathrm{d}t}\psi_n(t) = V_f'(\ell)\,(\psi_{n+1}(t) - \psi_n(t)) - V_{\mathrm{b}}'(\ell)\,(\psi_{n-1}(t) - \psi_n(t)). \tag{7}$$

Since the problem is linear, one can expand the solutions of (7) in a Fourier series. Each elementary plane wave solution of (7) is

$$\psi_n(t) = \mathrm{e}^{\mathrm{i}kn + z_k t}\tilde{\psi}, \tag{8}$$

where

$$k = \frac{2\pi}{N} j, \quad j = 0, \ldots, N-1 \tag{9}$$

is the wave number and z_k a complex frequency such that

$$\tau z_k^2 + z_k = V_-(\cos(k) - 1) + \mathrm{i}V_+ \sin(k), \tag{10}$$

where $V_\pm = V_{\mathrm{f}}'(\ell) \pm V_{\mathrm{b}}'(\ell)$.

If the real part $\mathrm{Re}(z_k)$ of z_k is larger than zero, the solution in (8) is unstable. We split z_k into its real and imaginary parts according to $z_k = p_k + \mathrm{i}\sigma_k$, where $p_k = \mathrm{Re}(z_k)$ and $\sigma_k = \mathrm{Im}(z_k)$. Insertion into (10) results in the two equations

$$\begin{aligned} \tau(p_k^2 - \sigma_k^2) + p_k &= V_-(\cos(k) - 1), \\ 2\tau p_k \sigma_k + \sigma_k &= V_+ \sin(k). \end{aligned} \tag{11}$$

Being interested in the threshold of stability, we need only to consider the case with $|p_k| \ll 1$ and hence we shall neglect terms of order $O(p_k^2)$ in solving equations (11). For σ_k, we obtain

$$\sigma_k = \frac{V_+ \sin(k)}{1 + 2\tau p_k} \approx V_+ \sin(k)(1 - 2\tau p_k). \tag{12}$$

Using the above approximate expression, we finally obtain the real part of z_k

$$p_k = \frac{2 \sin^2\left(\frac{k}{2}\right)}{1 + 4\tau^2 V_+^2 \sin^2(k)} \left(2\tau V_+^2 \cos^2\left(\frac{k}{2}\right) - V_-\right). \tag{13}$$

It is now easy to see that the free flow solution in (6) is linearly unstable for those k-values satisfying

$$\frac{2}{a} \frac{\left(V_\mathrm{f}'(\ell) + V_\mathrm{b}'(\ell)\right)^2}{V_\mathrm{f}'(\ell) - V_\mathrm{b}'(\ell)} \cos^2\left(\frac{k}{2}\right) > 1, \tag{14}$$

where the quantity $a = 1/\tau$ is the sensitivity. Note that this is an exact result. The inequality in (14) cannot be satisfied for any k if

$$a \equiv \frac{1}{\tau} > 2 \frac{\left(V_\mathrm{f}'(\ell) + V_\mathrm{b}'(\ell)\right)^2}{V_\mathrm{f}'(\ell) - V_\mathrm{b}'(\ell)}, \tag{15}$$

in which case the uniform traffic flow solution in (6) is always stable. For the OVs given by equations (4) and (5), the free flow solution is stable when

$$a > a_c, \tag{16}$$

where

$$a_c = \frac{2}{\cosh^2(\ell - b)} \frac{(f - b)^2}{f + b} \tag{17}$$

is the critical value of the sensitivity [25], and for the opposite inequality it is unstable with respect to the linear modes (8) with j satisfying the inequality

$$\frac{a_c}{a} \cos^2\left(\frac{\pi}{N} j\right) > 1. \tag{18}$$

In figure 2, we illustrate these instability regions. For a-values below the stability border lines, the free traffic flow is unstable and above it is stable. In each of these two cases, we present results from two different OV models, first $f = 1$ and $b = 0$, i.e. the simple and classical forward-oriented OV model and second $f = 1$, $b = 0.25$, i.e. the extended OV model, where the driver pays much more attention to the front car than to the rear car.

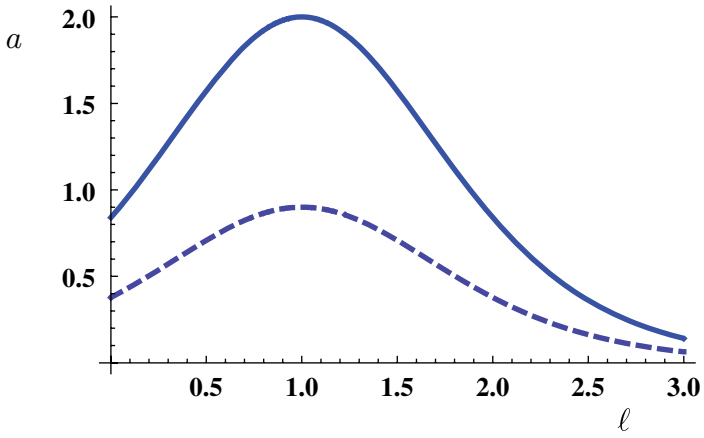

Figure 2. The phase diagram from equation (17) for two OV models. The solid line separates the area where the free flow is stable (above the curve) from the area where it is unstable (below the curve) in the forward-looking OV model ($f = 1, b = 0, h = 1$). The dashed line does the same in the case of forward–backward OV ($f = 1, b = 0.25, h = 1$).

4. Dynamics of the traffic jams: discrete modified KdV equation

In this section, we study non-uniform solutions, i.e. traffic jams and obtain the discrete modified KdV equation to describe the system.

From equations (2), (4) and (5) we obtain that the equations for the distance between the nearest cars

$$u_n(t) = s_{n+1}(t) - s_n(t) \tag{19}$$

have the form

$$\tau \ddot{u}_n + \dot{u}_n = f\ \tanh(u_{n+1} - h) + b\ \tanh(u_{n-1} - h) - f\ \tanh(u_n - h) - b\ \tanh(u_n - h). \tag{20}$$

Instead of u_n it is convenient to use the quantity w_n, which is defined by the equation

$$w_n = \tanh(u_n - h) \tag{21}$$

or

$$u_n = h + \frac{1}{2}\ \ln\left(\frac{1 + w_n}{1 - w_n}\right). \tag{22}$$

As it is seen from definition (21), w_n characterizes the deviation of the distance between neighbours from the safety distance between neighboring cars. Furthermore, w_n satisfies the periodicity condition

$$w_{n+N} = w_n. \tag{23}$$

Inserting equation (22) into (20), we obtain

$$\tau\ \frac{\mathrm{d}^2}{\mathrm{d}t^2} u_n + \frac{\mathrm{d}}{\mathrm{d}t} u_n = f(w_{n+1} - w_n) + b(w_{n-1} - w_n) \tag{24}$$

with u_n given by equation (22). Combining equations (2), (4), (5), (19) and (22) one can see that in terms of the new variables w_n the nth car position s_n can be expressed as follows:

$$s_n = hn + vt + \frac{1}{2}\sum_{n'=0}^{n-1} \ln\left(\frac{1+w_{n'}}{1-w_{n'}}\right). \tag{25}$$

It is worth noting that equation (24) is not of the gradient form. This means that there exists no functional $\mathcal{F}$ such that equation (24) can be written in the variational form $\delta\mathcal{F} = 0$. However, it is possible to separate in equation (24) the gradient part from the non-gradient one and present equation (24) as follows:

$$\frac{\mathrm{d}}{\mathrm{d}t} F'(w_n) - (f-b)\,\Delta_1 w_n = -\tau \frac{\mathrm{d}^2 u_n}{\mathrm{d}t^2} + \frac{f+b}{2}\,\Delta_2\, w_n, \tag{26}$$

where

$$\Delta_1 w_n \equiv \tfrac{1}{2}\,(w_{n+1} - w_{n-1})\,, \qquad \Delta_2 w_n \equiv w_{n+1} + w_{n-1} - 2\,w_n \tag{27}$$

are the discrete differential operators, and the function $F(w)$ is defined by the equation

$$F'(w) = \frac{1}{2}\,\ln\left(\frac{1+w}{1-w}\right). \tag{28}$$

The left-hand side of equation (26) can be presented in the gradient form

$$\frac{\mathrm{d}}{\mathrm{d}t} F'(w_n) - (f-b)\,\Delta_1 w_n = \frac{\delta\mathcal{L}}{\delta v_n}, \tag{29}$$

where the functional

$$\mathcal{L} = \sum_{n=1}^{N}\left(-F(\dot{v}_n) + \frac{f-b}{2}\,\dot{v}_n\,\Delta_1 v_n\right), \tag{30}$$

with $\dot{v}_n = (\mathrm{d}/\mathrm{d}t)v_n$ and the function v_n, given by the expression

$$w_n = \dot{v}_n, \tag{31}$$

plays a role of the Lagrangian and the right-hand side of equation (26) represents the non-gradient part of the system. By introducing a canonically conjugated momentum

$$p_n = \frac{\partial\mathcal{L}}{\partial\dot{v}_n} \tag{32}$$

and using the Legendre transformation

$$\mathcal{H} = \sum_{n=1}^{N} p_n\,\dot{v}_n - \mathcal{L} \tag{33}$$

one can obtain the Hamiltonian functional $\mathcal{H}$ in the form

$$\mathcal{H} = \sum_{n=1}^{N}\left(F(w_n) - w_n\,F'(w_n)\right). \tag{34}$$

It is straightforward to obtain from equations (26) and (34) with (23) that

$$\frac{\mathrm{d}\mathcal{H}}{\mathrm{d}t} = \sum_{n=1}^{N} \left[\tau\, w_n \frac{\mathrm{d}^2}{\mathrm{d}t^2} F'(w_n) + \frac{f+b}{2} (w_{n+1} - w_n)^2 \right]. \tag{35}$$

Considering equation (35) as an energy balance equation one can conclude that the second term in the right-hand side being definitely positive, represents a pumping of energy into the system while the first term gives an energy loss. This equation also suggests that in the steady state the right-hand side of equation (35) has to be zero.

Let us consider first the gradient part of the system that is described by the equation

$$\frac{\delta \mathcal{L}}{\delta v_n} = 0 \tag{36}$$

or equivalently by the equation

$$\frac{\dot{w}_n}{1 - w_n^2} - \frac{f-b}{2} (w_{n+1} - w_{n-1}) = 0. \tag{37}$$

This is the so-called discrete modified KdV equation. It is integrable and has been widely studied [27, 28]. We are interested in a traveling wave solution

$$w_n(t) = W(\kappa n + \omega t) \equiv W(\xi_n), \tag{38}$$

where ω is the frequency, κ is the wave number, $\xi_n = \kappa n + \omega t$ the traveling wave variable and therefore $c = \omega/\kappa$ is the wave train velocity, subject to the periodicity condition (23) or

$$W(\xi_{n+N}) = W(\xi_n). \tag{39}$$

5. Analytical traveling wave solution

In this section, we obtain analytical traveling wave solutions to equation (37) using the Sine–Gordon expansion method and it turns out to be convenient to approximate sums by integrals.

5.1. Non-uniform solutions

We will use the Sine–Gordon expansion method [29, 30] and present the solution of equation (37) in the form

$$W = A + \frac{\epsilon - A}{1 + B\, \mathrm{sn}(\xi\,|m)}, \tag{40}$$

where $\mathrm{pq}(u|m)(\mathrm{p,q} = \mathrm{c,n,d,s})$ denotes the Jacobi elliptic function, m is its modulus [31] and $\epsilon, \kappa, \omega, A, B$ are unknown coefficients. Inserting the traveling wave ansatz (40) into equation (37), we obtain algebraic equations for the unknown coefficients. They can be reduced to

$$\epsilon A = 1 - \bar{\omega} \frac{\mathrm{cn}(\kappa|m)\mathrm{dn}(\kappa|m)}{\mathrm{sn}(\kappa|m)}, \quad B = \frac{1}{\mathrm{sn}(\kappa|m)} \sqrt{1 - (1-\epsilon^2) \frac{\mathrm{sn}(\kappa|m)}{\bar{\omega}}}, \tag{41}$$

$$a_3\, \bar{\omega}^3 + a_2\, \bar{\omega}^2 + a_1\, \bar{\omega} + a_0 = 0, \tag{42}$$

where $\bar{\omega} = \omega/(f-b)$ is used and the coefficients $a_j (j = 0, 1, 2, 3)$ are given by

$$\begin{aligned} a_3 &= \mathrm{cn}^2(\kappa|m)\,\mathrm{dn}^2(\kappa|m), \\ a_2 &= \mathrm{sn}(\kappa|m)\left[1-(\mathrm{cn}(\kappa|m)\mathrm{dn}(\kappa|m)+1)^2+2\epsilon^2\mathrm{sn}(\kappa|m)\ \left(\mathrm{cn}^2(\kappa|m)+\mathrm{dn}^2(\kappa|m)\right)\right], \\ a_1 &= (1-\epsilon^2)\mathrm{sn}^2(\kappa|m)(1-\epsilon^2+2\mathrm{cn}(\kappa|m)\mathrm{dn}(\kappa|m)), \\ a_0 &= -(1-\epsilon^2)^2\mathrm{sn}^3(\kappa|m). \end{aligned} \tag{43}$$

Thus, the coefficients A and B and the frequency ω can be expressed in terms of the wave number κ and the parameter ϵ. From the periodicity condition (39), we obtain the wave number κ. It has the form

$$\kappa = \frac{4\,\mathbf{K}(m)}{N} j, \quad j = 1, 2, \ldots, \tag{44}$$

where $\mathbf{K}(m)$ is a complete elliptic integral of the first kind [33]. The unknown parameter ϵ can be obtained from the condition that the total length of all car distances is conserved:

$$\frac{1}{N}\sum_{n=1}^{N} u_n = \frac{L}{N}. \tag{45}$$

In the limit of $\epsilon \ll 1$ the frequency ω and the wave train profile $W(\xi)$ which are determined by equations (40)–(42), can be expressed as follows:

$$\frac{\omega}{f-b} = \mathrm{sn}(\kappa|m) - \epsilon^2\left(\frac{\mathrm{cn}(\kappa|m)-\mathrm{dn}(\kappa|m)}{1-\mathrm{cn}(\kappa|m)\,\mathrm{dn}(\kappa|m)}\right)^2 \mathrm{sn}(\kappa|m) + \mathcal{O}(\epsilon^4), \tag{46}$$

$$\begin{aligned} W = \sqrt{m}\,\mathrm{sn}(\kappa|m)\mathrm{sn}(\xi|m) + \epsilon\left(\frac{\mathrm{cn}(\kappa|m)-\mathrm{dn}(\kappa|m)}{1-\mathrm{cn}(\kappa|m)\mathrm{dn}(\kappa|m)}\right)^2 \mathrm{cn}(\kappa|m)\mathrm{dn}(\kappa|m) \\ -\epsilon\frac{m\mathrm{sn}^2(\kappa|m)}{1-\mathrm{cn}(\kappa|m)\mathrm{dn}(\kappa|m)}\,\mathrm{sn}^2(\xi|m) + \mathcal{O}(\epsilon^2). \end{aligned} \tag{47}$$

Inserting the traveling wave Ansatz (40) into equation (45), we obtain an equation that in principle gives the unknown quantity ϵ as a function of the other parameters. However, it is rather difficult to calculate sums containing elliptic functions. For the sake of simplicity in what follows we will assume that the wave profile is not very sharp and extend equation (40) by allowing n to be a continuum variable. This allows us to replace the sums by integrals and present equation (45) in the form

$$\frac{1}{8\mathbf{K}}\int_0^{4\mathbf{K}} \ln\left(\frac{1+W(\xi)}{1-W(\xi)}\right) \mathrm{d}\xi = \delta, \tag{48}$$

where the parameter $\delta = \ell - h$ gives the difference between the mean distance between neighboring cars and the safety distance. The periodicity condition (44) is also used. The function $\delta(\epsilon)$ that follows from equation (48) is presented in figure 3. An analytic dependence

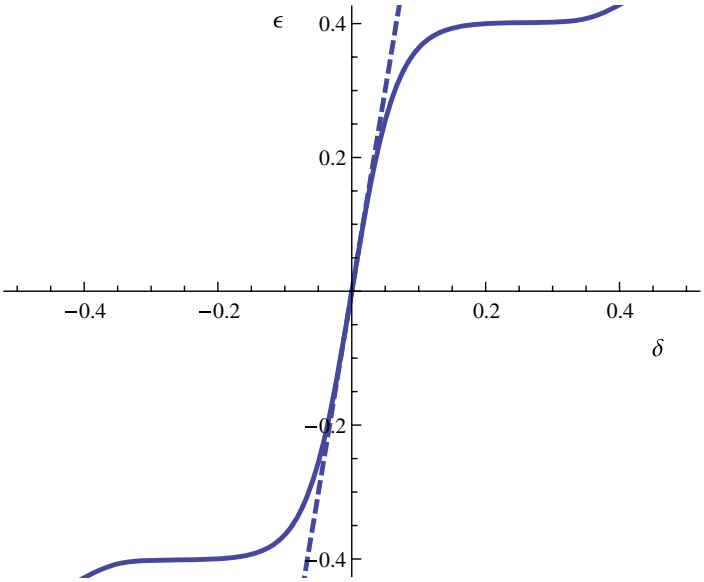

Figure 3. The figure shows the good approximation of equation (48) by equation (49) for small δ.

$\delta(\epsilon)$ may be obtained from equation (48) for small ϵ (which as it is seen below corresponds to $|\delta| < 1$). It has the form

$$\epsilon = \delta \frac{(1 - \mathrm{cn}(\kappa, m)\mathrm{dn}(\kappa, m))\mathbf{K}(m)}{\mathbf{K}(m) - \mathrm{cn}(\kappa, m)\mathrm{dn}(\kappa, m)\mathbf{\Pi}(n, m)}, \tag{49}$$

where $\mathbf{\Pi}(n, m)$ with $n = m\mathrm{sn}^2(\kappa|m)$ is the elliptic integral of the third kind [31]. Figure 3 shows also that the dependence (49) gives a rather accurate description in the interval of its applicability.

Combining equations (22) and (47), we can conclude that in the case when the mean distance ℓ coincides with the safety distance h the headways $u_n \equiv s_{n+1} - s_n$ in jam and rarefaction regions change in a symmetric way with respect to the car index (see figure 4(a)) while for $\delta > 0$ the length of the jam region is smaller than the rarefaction region (see figure 5). The symmetric profile shown in figure 4(a) is asymmetric in the density plot over space, shown in figure 4(b). The density ϱ is defined at discrete positions s_n by $\varrho(s_n) = 2/(u_n + u_{n-1})$. The numerical results also shown in figure 4 will be discussed in section 6.

5.2. *Stability of the non-uniform solution*

The traveling wave solution (40)–(42) was obtained by neglecting the non-gradient terms in equation (26) (i.e. the right-hand side of equation (26)). In this section, we give an additional argument showing that the non-gradient terms do not affect the traveling wave solution. In this sense it is a stable solution of the system (26). To show this, we apply the method of collective coordinates widely used in different areas of nonlinear science [32]. The trial function is the traveling wave solution (40)–(42) and the modulus m is a time-dependent variational parameter. Due to the periodicity condition (39) the modulus also depends on the wave number $\kappa(j)$ $(j = 1, 2, \ldots, N)$. The evolution of the modulus $m(t)$ is given by the energy balance

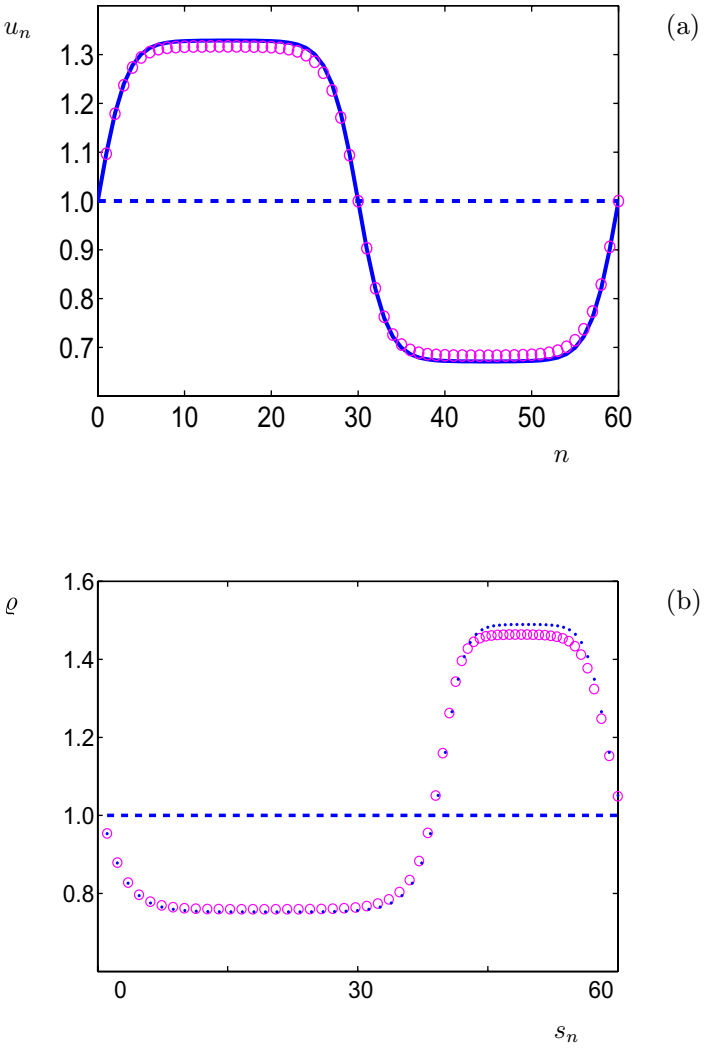

Figure 4. (a) The distance u_n between neighboring cars versus the car number n. The dashed line corresponds to the equidistant uniform car flow, the solid curve corresponds to the analytical solution of a situation with a jam area and a free flow area. There is excellent agreement with the numerical results plotted as circles (refer to section 6). The solid line is obtained from equations (22) and (40)–(42) with $\ell = h = 1$, $\tau = 0.52$ and $N = 60$. The practical procedure to obtain the graph of the analytical results for finite N is as follows. First one fixes the modulo as $m = 1/(1+\exp(-p))$ which is close to 1 for $p > 5$. Using equation (54) one calculates κ. Since the fixed point is given by $Q(m) = 0$ one can determine τ from equations (59) and (60) such that $G(m) = L(m)$. For the current plot with $N = 60$ cars, we used $p = 6.75$, which leads to $m = 0.9988$ and finally to $\tau = 0.52$. (b) Plot of the density $\varrho(s_n) = 2/(u_n + u_{n-1})$ over the position s_n of car n. Also here is excellent agreement between the analytical findings plotted as small blue dots and the numerical results plotted as circles.

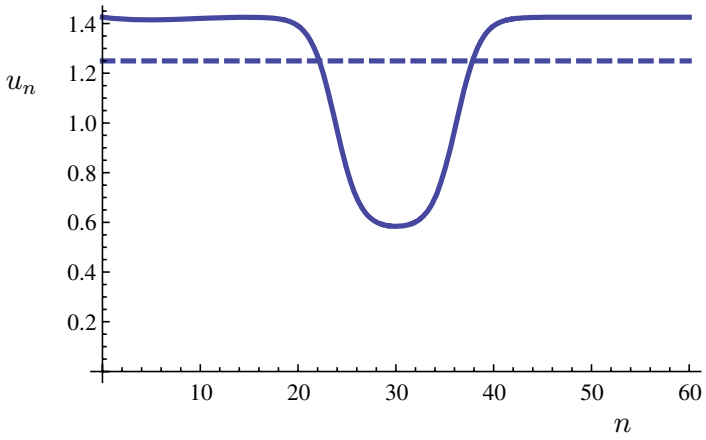

Figure 5. As in figure 4, we consider $N = 60$ cars but now on a ring with $L = 75$, thus $\ell = 1.25$. However, the safety distance $h = 1$ is still used in the OV function. The dashed line describes the equidistant uniform car flow, the solid curve corresponds to the analytical solution with a jam area and a free flow area.

equation (35), which in the continuum limit is

$$\frac{\mathrm{d}\mathcal{H}}{\mathrm{d}t} = G - L, \tag{50}$$

where

$$\mathcal{H} = \frac{1}{4\mathbf{K}} \int_0^{4\mathbf{K}} \Big[F(W) - W\, F'(W) \Big] \mathrm{d}\xi \tag{51}$$

is a continuum version of the Hamiltonian (34) and the terms

$$G = \frac{f+b}{2} \frac{1}{4\mathbf{K}} \int_0^{4\mathbf{K}} W(\xi) \Big[2\, W(\xi) - W(\xi+\kappa) - W(\xi-\kappa) \Big] \mathrm{d}\xi \tag{52}$$

and

$$L = \tau\, \omega^2 \frac{1}{4\mathbf{K}} \int_0^{4\mathbf{K}} \frac{1}{1 - W^2(\xi)} \left(\frac{\mathrm{d}W}{\mathrm{d}\xi} \right)^2 \mathrm{d}\xi \tag{53}$$

describe the energy gain and loss, respectively.

For the sake of simplicity, we restrict ourselves to the case when $\ell = h$ or equivalently, to $\epsilon = 0$ (see equation (49)). In this case, as it is seen from equations (46) and (47), the traveling wave ansatz is determined by the expression

$$\omega = (f - b)\, \mathrm{sn}(\kappa|m), \quad W(\xi) = W_m\, \mathrm{sn}(\xi|m), \quad \kappa = \frac{4\,\mathbf{K}(m)}{N}\, j,\ j = 1, 2, \ldots \tag{54}$$

with $m = m(t)$. Here

$$W_m = \sqrt{m}\, \mathrm{sn}(\kappa|m) \tag{55}$$

is the wave front amplitude that characterizes the change in the distance between neighboring cars in the jam region with respect to the free flow state. Introducing equation (54) into (50)

after some calculations, we obtain that the dynamics of the modulus $m(t)$ is governed by an equation that has the form of an equation of motion for an overdamped oscillator

$$\gamma(m)\,\dot{m} = Q(m), \tag{56}$$

where

$$\gamma(m) = -\frac{1}{2}\frac{\mathrm{d}}{\mathrm{d}m}\frac{1}{\mathbf{K}}\int_0^{\mathbf{K}} \ln\left(1 - m\,\mathrm{sn}^2(\kappa|m)\,\mathrm{sn}^2(\xi|m)\right)\,\mathrm{d}\xi \tag{57}$$

is an effective damping and

$$Q(m) = L(m) - G(m), \tag{58}$$

with

$$G(m) = (f+b)\left[-\mathrm{sn}^2(\kappa|m)\mathbf{E}(m) + \mathrm{sn}^2(\kappa|m)\mathbf{K}(m) + \mathrm{cn}(\kappa|m)\mathrm{dn}(\kappa|m)\,(\mathbf{K}(m) - \mathbf{\Pi}(n,m))\right] \tag{59}$$

and

$$L(m) = \tau\,(f-b)^2\left[\mathrm{sn}^2(\kappa|m)\mathbf{E}(m) - \mathrm{dn}^2(\kappa|m)\mathbf{K}(m) + \mathrm{cn}^2(\kappa|m)\mathrm{dn}^2(\kappa|m)\mathbf{\Pi}(n,m)\right] \tag{60}$$

is an effective force, where $\mathbf{E}(m)$ is an elliptic integral of the second kind [31]. The equation

$$Q(m) = 0 \tag{61}$$

gives the position of the fixed points. Expanding the elliptic functions in equations (57)–(60) for $m \ll 1$ one obtains

$$\gamma(m) = \frac{1}{2}\,\sin^2\left(\frac{2\pi}{N}\,j\right),$$

$$Q(m) = \frac{1}{2}\,(f+b)\,\sin^2\left(\frac{2\pi}{N}\,j\right)\sin^2\left(\frac{\pi}{N}\,j\right)\left[\frac{a_c}{a}\,\cos^2\left(\frac{\pi}{N}\,j\right) - 1\right] m. \tag{62}$$

Thus, the stability of the fixed point $m = 0$ for equation (56) coincides with the stability condition (16) of the free flow. When

$$a < a_c, \tag{63}$$

the fixed point $m = 0$ is unstable for those j for which $Q'(0) > 0$. In this case, a new fixed point m_w (with $m_w \neq 0$) appears. This fixed point corresponds to a stable wave train of finite amplitude. It is impossible to obtain an explicit expression for this fixed point in a general case. However, taking into account that for $N \to \infty$, $m_w \to 1$, for $N \gg 1$ and m close to 1 one can obtain that

$$Q(m) = (f+b)\,\mathrm{sn}(\kappa|m)\left\{\frac{1}{2}\left(\frac{a_c}{2a} + \mathrm{cn}^2(\kappa|m)\right)\ln\left(\frac{1+\mathrm{sn}(\kappa|m)}{1-\mathrm{sn}(\kappa|m)}\right) - \left(\frac{a_c}{2a}+1\right)\mathrm{sn}(\kappa|m)\right\} \tag{64}$$

and the solution $m_w = m_w(a, N)$ of equations (61) and (64) for $j = 1$ is determined as an implicit function

$$\mathrm{sn}\left(\frac{4\,\mathbf{K}}{N}\middle| m\right) - \sqrt{5\left(\frac{a_c}{a} - 1\right)} = 0. \tag{65}$$

Equations (44), (46) and (61) give a parametric dependence of the wave front velocity

$$c = \frac{\omega}{\kappa} \equiv (f-b)\,\frac{\mathrm{sn}(\kappa|m)}{\kappa} \tag{66}$$

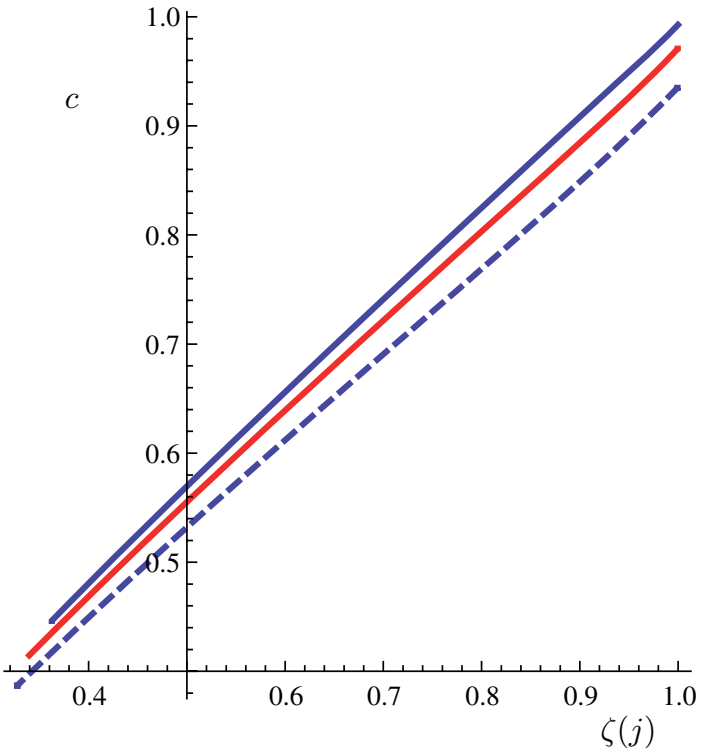

Figure 6. The velocity of the front c versus the relative sensitivity $\zeta(j)$ ($N = 30$) for three different values of the number of jams: $j = 1$ (blue line), $j = 2$ (red line) and $j = 3$ (dashed line).

on the relaxation time τ, attention parameters f, b and the number of jams j. The velocity of the nth car can be obtained by combining equations (25) and (40). It has the form

$$\dot{s}_n = v + \frac{c}{2} \ln\left(\frac{1 + W(\kappa n + \omega t)}{1 - W(\kappa n + \omega t)}\right). \tag{67}$$

Taking into account equations (54) and (66) one can conclude from equation (67) that for $f > b$ (the driver pays more attention to the front car than to the rear car) the cars in the rarefaction region where $W(\kappa n + \omega t) > 0$ move faster than in the jam region, where $W(\kappa n + \omega t) < 0$. In the case when $f < b$, the cars that belong to the rarefaction regions move slower than the cars in the region with $W(\kappa n + \omega t) < 0$. While the travel direction of the cars is counterclockwise, the wave fronts that separate the rarefaction and jam regions move clockwise when $f > b$ and counterclockwise when $f < b$. Alternatively, one can obtain this result by determining the sign of c in equation (66) with the sign of $f - b$ because $\mathrm{sn}(\kappa|m)\kappa$ is always positive due to equation (65).

The dependence of the velocity c on the relative sensitivity

$$\zeta(j) = \frac{a}{a_c \cos^2(j(\pi/N))} \tag{68}$$

for different values of the number of jams j is presented in figure 6. As it is seen from figure 6, the wave front velocity c increases almost linearly as the relative sensitivity $\zeta(j)$ increases. The wave front amplitude W_m given by equation (55) with the modulus m determined from

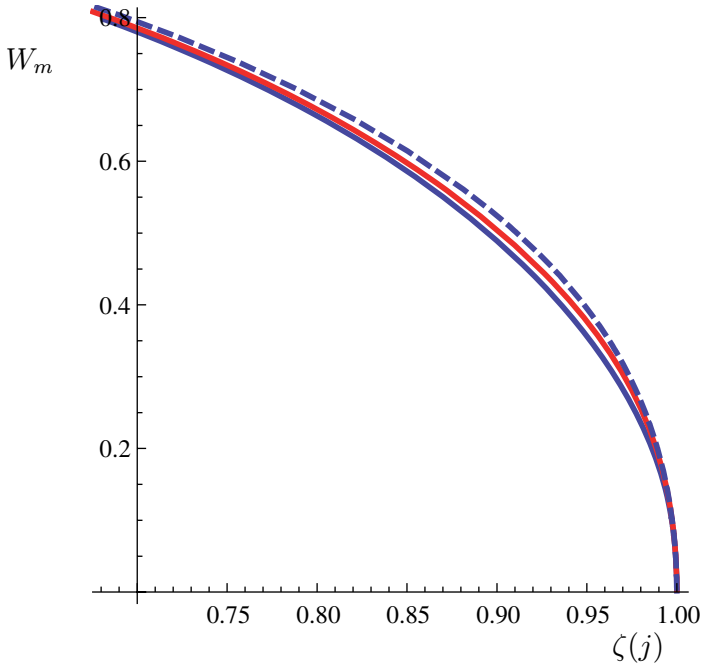

Figure 7. The wave front amplitude W_m versus the relative sensitivity $\zeta(j)$ for three different values of the number of jams: $j = 1$ (blue line), $j = 2$ (red line) and $j = 3$ (dashed line). See equation (55).

equation (61) as a function of the relative sensitivity for different values of the number of jams j is presented in figure 7.

6. Numerical studies

To verify our results, we have performed several numerical studies. A Runge–Kutta solver is used to solve the equations (20) numerically under the index boundary conditions

$$u_{n+N} = u_n. \tag{69}$$

The numerical results are in very good agreement with the analytical ones, which was already shown in figure 4. The profile u_n over the car index n is symmetric as is shown in figure 4(a) while the density plot over space is asymmetric, which is shown in figure 4(b). As was already mentioned, the density ϱ is defined at discrete positions s_n by $\varrho(s_n) = 2/(u_n + u_{n-1})$.

We investigated initial values that result in different numbers of jam regions in the traffic flow. Considering solutions to equations (20) for the sensitivity a in the interval $1 < (a_c/a) < 1 + \eta$ ($\eta \ll 1$) the free flow is in accordance with the linear stability analysis unstable with respect to the linear modes with small wave number k.

For the used initial values, using the same set of parameters, the system evolves either to a state with one jam area or two jam areas. A time evolution for the number of cars $N = 60$ and $a_c/a = 1.04$ is shown in figure 8. Here, we use two initial seeds

$$u_n(0) = 1 + \mu \sin\left(\frac{2\pi}{N} n\right) \tag{70}$$

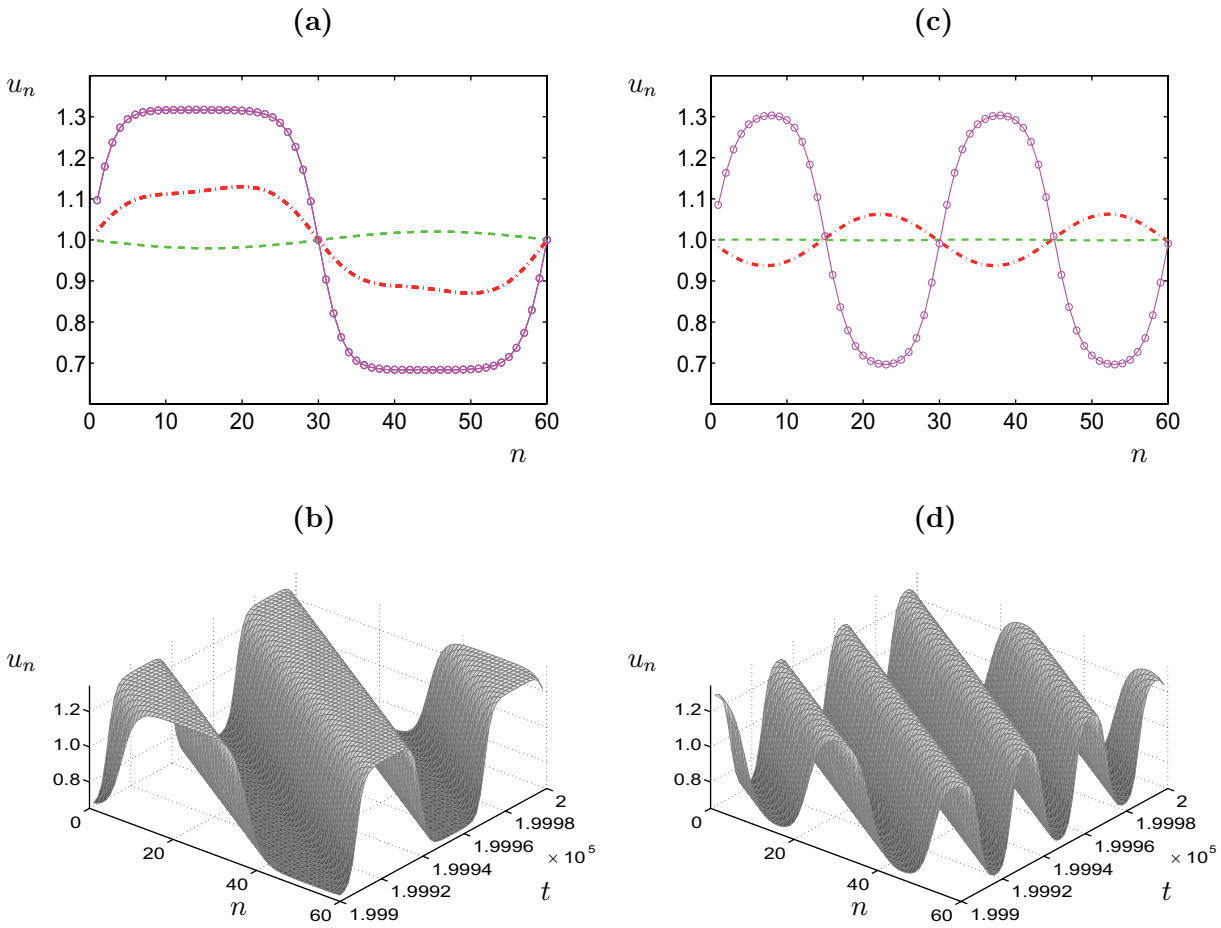

Figure 8. (a, b) The evolution of the distance between neighboring cars u_n obtained from the results of numerical simulations of equation (20) with initial value (70) and $\mu = 10^{-3}$ for $f = 1, b = 0, \ell = h = 1$, the relaxation time $\tau = 0.52$ and $N = 60$. The parameter values correspond to the unstable region and hence the nearly equidistant spacing between cars emerges into the formation of traffic jams. (a) Snapshots for $t = 1500$ (dashed line), $t = 25\,000$ (dashed dotted line), $t = 200\,000$ (line with circles). (b) Time evolution for $199\,900 < t < 200\,000$ for the initial condition given by equation (70). (c, d) The same for the initial condition given by equation (71). (c) Snapshots for $t = 0$, $t = 7000$ (dashed dotted line) and $t = 200\,000$ (line with circles).

and

$$u_n(0) = 1 + \mu \sin\left(\frac{4\pi}{N} n\right), \tag{71}$$

respectively. The upper panels in these figures give the flow profile for three different initial values. It is seen that in a full accordance with the analysis for the seed (70) a one-jam pattern is formed while for the seed (71) there appear two jam regions. Figure 8(b) and (d) show that the jam regions propagate along the flow with a constant velocity, preserving their shape.

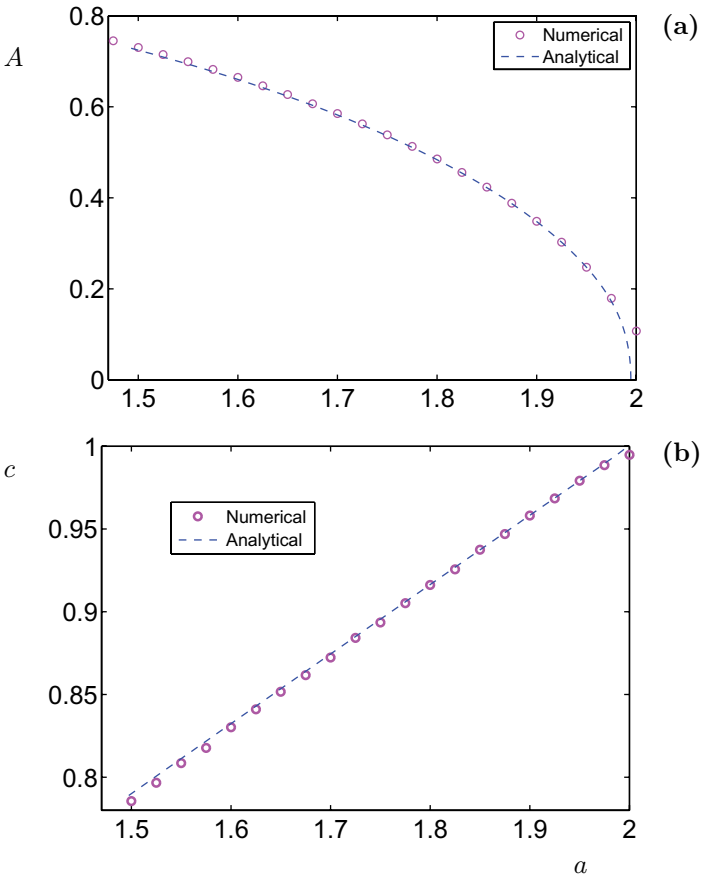

Figure 9. (a) Comparison of the analytically obtained dependence of the wave front amplitude A on the sensitivity a with the results of numerical simulations. (b) Comparison of the analytically obtained dependence of the wave front velocity c on the sensitivity a with the results of numerical simulation. For the analytical relationship, we use equations (44) and (46) to get ω and k and hence the wave velocity c. With the numerical simulation we measure how fast the centroid position of a density pulse moves backwards. Parameters used: $N = 60$, $f = 1$, $b = 0$, $\ell = h = 1$ and $\mu = 0.1$ for the initial value (70).

The comparison of analytically and numerically obtained dependencies of the amplitude W_m and the velocity c of the wave front on the sensitivity a is presented in figure 9. We performed several numerical simulations with $N = 60$ where we investigated parameter values for sensitivities $a \in [1.5, 2]$. The numerical values for A and c, we obtain by simulating the original system given in equation (2) for a sufficiently long time until a stable density pulse developed at $t = 15\,000$. We checked that the amplitude A remained stationary. As the initial condition for the simulations we used again equation (70), which is a slight harmonic distortion of the uniform flow situation ($u_n = \ell$). While by $u_n(0)$ the initial car positions are defined we fix the remaining degrees of freedom by setting $\dot{s}_n = V(\ell)$, i.e. the initial velocities of the cars correspond to the uniform flow. Running the numerical simulations for $t = 15\,000$ results in a transformation of the density profile from the initial harmonic seed to a typically sharp density profile (close to the solitonic limit i.e. m is very close to 1).

The amplitude A we determine numerically directly from the maximal u_n. In order to estimate the wave velocity c numerically, we calculate the centroid of the density pulse. As mentioned, we can safely claim that after $t = 15\,000$ a stable density pulse emerges for the given parameter interval $a \in [1.5, 2]$. In fact, the amplitude A becomes stationary much earlier. Thus we can compare the density pulse at $t = 14\,000$ with the pulse at $t = 15\,000$ and estimate the velocity c by comparing the centroid positions. These numerical estimates are in good accordance with the analytically obtained wave velocity given by equation (66), as can be seen in figure 9.

7. Conclusions

In this paper, we studied car traffic numerically and analytically on a closed loop using a follow-the-leader model. An extended version of the OV model was considered where a driver takes into account both the following car and the preceding car and the classical forward-looking OV model is contained as a special case. The system has a homogeneous solution (free flow) that destabilizes for long waves as driver forward sensitivity increases. Then the solution is a periodic wave train of jam and rarefaction regions.

To understand this effect we analyzed the equation of motion. We split it into a gradient part which is the variational derivative of a functional and a non-gradient part. The gradient part is the so-called discrete modified KdV equation which is completely integrable. This equation has exact periodic wave train solutions. The non-gradient terms do not affect this solution. We show that it is a stable limit cycle of the system in the sense that its parameter varies as for an overdamped oscillator. These periodic solutions are in excellent agreement with the numerical solutions of the traffic flow equations both for the amplitude and velocity of the jam wave. Different unstable wave numbers have been tested and agreement remains. An important observation is that the velocity of the jam region monotonically increases when the sensitivity increases.

A practical consequence of this study is that for a given set of parameters, number of cars, length of the route and forward and backward driver sensitivity, one can estimate the most unstable wave numbers. Then for each one of these one can compute the amplitude and extension of the traffic jams and their speed.

Acknowledgments

The authors thank Toyota Central R&D Labs, Japan for financial support. Yu G acknowledges the Department of Mathematics at the Technical University of Denmark and the Laboratoire de Mathématiques, INSA de Rouen, France for Guest Professorships. He is thankful to the Department of Mathematics, Technical University of Denmark for its hospitality. Yu G acknowledges also partial support from a special program of the National academy of sciences of Ukraine.

References

[1] Wolf D E, Schreckenberg M and Bachem A (ed) 1996 *Traffic and Granular Flow* (Singapore: Word Scientific)
[2] Helbing D 2001 *Rev. Mod. Phys.* **73** 1067
[3] Nagatani T 2002 *Rep. Prog. Phys.* **65** 1331

[4] Kerner B 2004 *The Physics of Traffic* (Berlin: Springer)
[5] Chowdhury D, Santen L and Schadschneider A 2000 *Phys. Rep.* **329** 199
[6] Nagel K, Wagner P and Woesler R 2003 *Oper. Res.* **51** 1
[7] Wagner P and Nagel K 2008 *Eur. Phys. J.* B **63** 315
[8] Bando M, Hasebe K, Nakayama A, Shibata A and Sugiyama Y 1995 *Phys. Rev.* E **51** 1035
[9] Berg P, Mason A and Woods A 2000 *Phys. Rev.* E **61** 1056
[10] Lee H Y, Lee H-W and Kim D 2001 *Phys. Rev.* E **64** 056126
[11] Lee H Y, Lee H-W and Kim D 2004 *Phys. Rev.* E **69** 016118
[12] Nagel K and Schreckenberg 1992 *J. Physique* **2** 2221
[13] Kerner B S and Konhäuser P 1993 *Phys. Rev.* E **48** 2335
[14] Kurtze D A and Hong D C 1995 *Phys. Rev.* E **52** 218
[15] Komatsu T and Sasa S 1995 *Phys. Rev.* E **52** 5574
[16] Ou Z-H, Dai S-Q and Dong L-Y 2006 *J. Phys. A: Math. Gen.* **39** 1251
[17] Nakanishi K, Itoh K, Igarashi Y and Bando M 1997 *Phys. Rev.* E **55** 6519
[18] Mason A D and Woods A W 1997 *Phys. Rev.* E **55** 2203
[19] Bando M, Hasebe K, Nakanishi K and Nakayama 1998 *Phys. Rev.* E **58** 5429
[20] Huijberts H J C 2002 *Phys. Rev.* E **65** 471031
[21] Igarashi Y, Katsumi I, Nakanishi K, Ogura K and Yokokawa K 2001 *Phys. Rev.* E **64** 047102
[22] Gasser I, Sirito G and Werner B 2004 *Physica* D **197** 222
[23] Orosz G, Krauskopf B and Wilson R E 2005 *Physica* D **211** 277
[24] Hayakawa H and Nakanishi K 1998 *Prog. Theor. Phys. Suppl.* **130** 57
[25] Nakayama A, Sugiyama Y and Hasebe K 2002 *Phys. Rev.* E **65** 016112
[26] Ge H X, Zhu H B and Dai S Q 2006 *Eur. Phys. J.* **54** 503
[27] Wadati M 1975 *J. Phys. Soc. Japan* **38** 673
[28] Ablowitz M A and Ladik J F 1976 *J. Math. Phys.* **17** 1011
[29] Yan Z 2006 *Nonlinear Anal.* **64** 1798
[30] Fan X and Lu T 2007 *Int. J. Nonlin. Sci.* **3** 52
[31] Abramowitz M and Stegun I 1972 *Handbook of Mathematical Functions* (New York: Dover)
[32] Scott A 2003 *Nonlinear Science—Emergence and Dynamics of Coherent Structures* (Oxford: Oxford University Press)
[33] Gradshteyn I S and Ryzhik I M 1980 *Table of Integrals, Series and Products* (New York: Academic)